Variation in rising limb of Colorado River snowmelt runoff hydrograph controlled by dust radiative forcing in snow

Thomas H. Painter[1], S. McKenzie Skiles[2], Jeffrey S. Deems[3], W. Tyler Brandt[4], and Jeff Dozier[4]

[1]Jet Propulsion Laboratory, California Institute of Technology, Pasadena, CA, 91109 USA.
[2]Department of Geography, University of Utah, Salt Lake City, UT, 84112 USA.
[3]National Snow and Ice Data Center, University of Colorado, Boulder, CO, 80309 USA.
[4]Bren School of Environmental Science & Management, University of California, Santa Barbara, CA, 93106-5131.

Corresponding author: Thomas H. Painter (thomas.painter@jpl.nasa.gov)

Key Points:

- Radiative forcing by dust on snow controls the interannual variability in the shape of the rising limb of the snowmelt hydrograph
- The rising limb's average steepness and the statistical distributions of its 1st and 2nd derivatives define its shape
- Variability in the rising limb's shape is independent of air temperature

This article has been accepted for publication and undergone full peer review but has not been through the copyediting, typesetting, pagination and proofreading process which may lead to differences between this version and the Version of Record. Please cite this article as doi: 10.1002/2017GL075826

Abstract

Common practice and conventional wisdom hold that fluctuations in air temperature control interannual variability in snowmelt and subsequent river runoff. However, recent observations in the Upper Colorado River Basin confirm that net solar radiation and by extension radiative forcing by dust deposited on snow cover exerts the primary forcing on snowmelt. We show that the variation in the shape of the rising limb of the annual hydrograph is controlled by variability in dust radiative forcing and surprisingly is independent of variations in winter and spring air temperatures. These observations suggest that hydroclimatic modeling must be improved to account for aerosol forcings of the water cycle. Anthropogenic climate change will likely reduce total snow accumulations and cause snowmelt runoff to occur earlier. However, dust radiative forcing of snowmelt is likely consuming important adaptive capacity that would allow human and natural systems to be more resilient to changing hydroclimatic conditions.

Plain Language Summary

We address the question, do air temperatures or absorbed solar radiation explain the year-to-year variability of the rate of snowmelt, and therefore the shape of the way the streamflow rises in the melt season? Our analysis shows that absorbed solar radiation, which varies with the amount of wind blown dust deposited into the snowpack, causes the streams to rise more quickly in years with more dust, whereas the rate at which the streams rise does not depend on air temperature. Forecasts of snowmelt runoff must account for the variability in dust deposition.

1 Introduction

Worldwide, snowmelt and glaciers provide water resources for about two billion people (Mankin et al., 2015), and snow and glacier melt in the mountains supply most of the agricultural and urban water resources for at least a billion (Barnett et al., 2005). In mountain ecosystems, snowmelt sustains soil moisture late into the melt season. Thus, the timing and magnitude of snowmelt rates control the timing and rates of river discharge, which in turn influence water availability, flood potential, hydroelectric generation, and water quality. In the Western US, intense water management through vast reservoir operations relies on extensive point measurements for monitoring and predicting weekly to seasonal snowmelt runoff. Even in this region where the snowpack and water supply are closely monitored, runoff forecasting errors often reach 40% during the rising limb of the hydrograph (Bryant et al., 2013).

In the world's great mountain ranges, such as High Mountain Asia, sparse monitoring of water and the snowpack supports little predictive capability. Combined with relatively few reservoirs, the timing of runoff directly dictates water availability and immediate flood potential. Understanding the physical controls on variation in the timing and magnitude of snowmelt runoff is key to improved simulation and forecasting, and for more accurate projection of the changes in water resources under a changing climate.

1.1 Streamflow

Streamflow in most snowmelt-dominated mountain systems follows a typical seasonal pattern: low flow in the fall and winter months, snowmelt surge in spring, peak flow in mid to late spring, followed by a slow recession to baseflow (Dunne & Leopold, 1978). Variation in streamflow rates from base flow to peak flow is governed by the surface energy balance and subsequent generation of melt water from the mountain snowpack. Faster snowmelt and a

shorter rise to peak flow compress the time interval over which daily to seasonal operational water supply and flood control decisions are made. A steeper hydrograph can exhibit a 'flashy' behavior, complicating identification of the actual snowmelt peak, the timing of which is frequently used to make decisions about water management or allocate water rights (Kenney et al., 2008).

1.2 Snow energy balance

Approaches to snowmelt runoff modeling have generally depended on the relatively weak, empirical positive relationship between melt and temperature, an approach encouraged by the relative abundance of temperature measurements and the lack of measurements of other energy fluxes (Hock, 2003, 2005). However, estimates of melt from temperature alone depend on time- and space-varying *melt factors* or *degree-day factors* that attempt to balance positive and negative errors but do not explicitly address driving processes (Hock, 2003; Kumar et al., 2013). These factors in effect index the relative contributions of energy flux components to melt production, and therefore are site- and year-dependent. These calibrated relationships between temperature and snowmelt are likely to suffer even greater errors under a changed energy balance regime, whether caused by climate warming or by other forcings such as dust or black carbon (Dozier, 2011; Milly et al., 2008). Seasonally-varying melt factors are commonly applied, recognizing implicitly that the melt energy/air temperature relationship is not constant throughout the snowmelt season. Additional radiation components have been added to some temperature-index models but with inconsistent subsequent adoption (Brubaker et al., 1996; Kustas & Rango, 1994).

While increasing temperatures have the potential to push snowmelt timing earlier in the year, the need for forecasting systems that are resilient to changing environmental conditions demands that we reconcile interannual variability in snowmelt runoff with the physical controls on snowmelt (Blöschl, 1991; Kirnbauer et al., 1994; Marks & Dozier, 1992; Oerlemans, 2000). Our general understanding of physical processes illustrates that, except for snowpacks under the densest tree canopies or lying in deep cirques, net solar radiation (governed by varying irradiance and albedo) dominates the contribution to melting energy (Marks & Dozier, 1992; Oerlemans, 2000; Painter et al., 2007; Van den Broeke et al., 2011). For example, across the melt seasons in three years on the Morteratschgletscher, Switzerland, net solar radiation contributed 93% of the net energy flux in the snowpack (Oerlemans, 2000). In Greenland, where solar elevation angles are smaller, net solar radiation is the dominant source of energy for surface melt (Box et al., 2012; Tedesco et al., 2011; Van den Broeke et al., 2011). In the San Juan Mountains of Colorado (Figure 1), net solar radiation also dominates the energy balance during periods of melt (Painter et al., 2007; Painter et al., 2010; Skiles et al., 2012). When offset by the negative net longwave flux, the net allwave radiation contributes 99% of the energy available for melt (Figure S1). The large variation in snow albedo driven by variations in dust deposition, concentrations, and exposure drive large variation in net radiation and thereby snowmelt rates [*Painter et al.*, 2012, *Skiles et al.*, 2012].

Changes in albedo in different parts of the solar spectrum depend primarily on changes in snow grain size and impurity concentrations. When snow grains grow through wet snow metamorphism, reflectance drops mainly in the near-infrared wavelengths (0.8 to 1.5 μm) (Wiscombe & Warren, 1980). However, dust and black carbon lower the reflectivity primarily in the visible spectrum (Figure 1) because the absorption coefficients for dust or black carbon are orders of magnitude greater than for ice in these wavelengths (Warren & Wiscombe, 1980; Warren & Brandt, 2008). The dust and carbon particles absorb sunlight and cause a *direct* feedback by accelerating snowmelt and metamorphism; the associated grain

growth and lower near-infrared albedo from this acceleration is the *indirect* feedback (Hansen & Nazarenko, 2004; Skiles et al., 2012).

In mountain regions that receive strong loading of dust and black carbon to snow and ice, such as the Colorado Rockies (Painter et al., 2007; 2012b; Skiles et al., 2012), Alps (Painter et al., 2013a), Hindu Kush-Himalaya (Kaspari et al., 2011; 2014; Nair et al., 2013; Thompson et al., 2000; Yasunari et al., 2013), and Caucasus Mountains (Davitaya, 1969), enhanced absorption of sunlight increases snowmelt rates markedly. Therefore, simulations that rely on air temperature to diagnose changes in snow and ice melt in regions susceptible to high impurity loading will frequently struggle to predict melt and runoff timing and magnitude (Bryant et al., 2013).

Here we investigate the basin-scale controls on the shape of the rising limb of the runoff hydrograph of rivers in the San Juan Mountains, Colorado. The rate at which the river rises from baseflow to its peak discharge varies from year to year, driven by energy-balance controlled snowmelt rates. Our physical understanding of snowmelt processes suggests that the slope of the hydrograph rising limb should therefore be determined primarily by net solar input, and by air temperature to a much lesser degree. In this paper we test this assertion; to what degree is interannual variability in steepness of the rising limb of these hydrographs controlled by (i) variability in winter and spring air temperature, and (ii) variability in dust radiative forcing in snow.

2 Materials and Methods

2.1 Site description

Despite the long duration of observations and reconstructions of runoff in the Colorado River Basin (Hamlet et al., 2005; Woodhouse et al., 2006), the first comprehensive measurements of snow surface energy balance and detailed radiation in the Upper Colorado began in 2005 in the San Juan Mountains of Colorado (Landry et al., 2014; Painter et al., 2007). These data reveal that radiative forcing from regional dust shortens duration of the mountain snow cover by 20-50 days (Painter et al., 2007; 2012b; Skiles et al., 2012). The current annual level of dust deposition is 5-7 times greater than it was prior to the widespread disturbance of the Colorado Plateau and Great Basin in the mid-1800s (Neff et al., 2008), and appears to have increased during the ongoing 15-year drought (Brahney et al., 2013; Skiles et al., 2012). The extrapolation of these forcings to the entire Upper Colorado River Basin with a hydrologic model suggests that the peak runoff at the basin midpoint Lee's Ferry comes more than 3 weeks earlier and with an average of 5% less flow than prior to the disturbance of the western deserts (Deems et al., 2013; Painter et al., 2010).

(a)

(b)

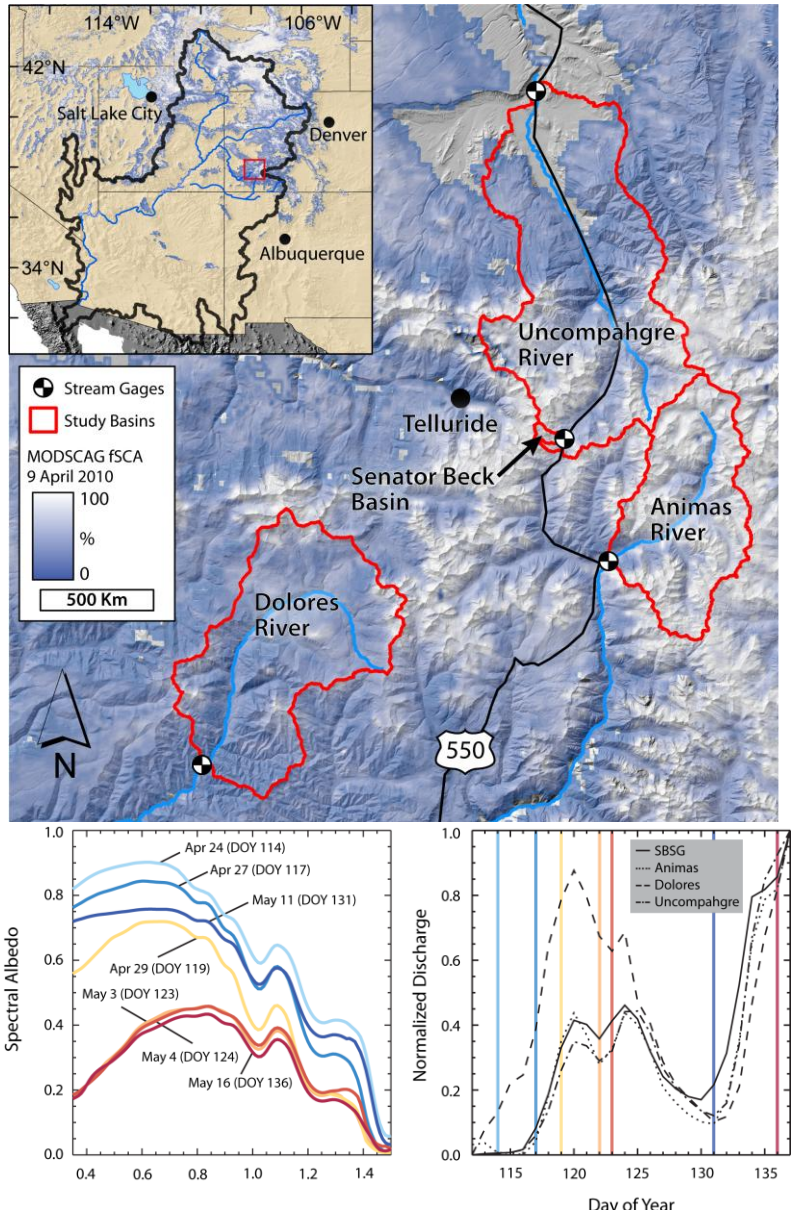

Figure 1. (**a**) Overview of the San Juan Mountains in the eastern half of the Colorado River Basin, the Senator Beck Basin Study Area, and the studied rivers: Uncompahgre, Animas, and Dolores. (**b**) Spectral albedo of snow at the energy balance tower site during various dates along the rising limb of the hydrograph in 2013, with those dates color highlighted on the rising limb in Figures 2 and 3. SBSG is the Senator Beck Stream Gage at the outlet of the basin. The base map for snow covered area (MODSCAG f_{SCA}) comes from the NASA MODIS Snow Covered Area and Grain size (MODSCAG) model (Painter et al., 2009) and we use 9 April 2010 data simply to show the extent of snow at near maximum coverage.

In simulations across 2005-2010 in this region, air temperature increases of 2°C and 4°C increased daily mean longwave irradiance by averages of 8 W m^{-2} and 16 W m^{-2}, and increased daily mean sensible heating by about 2 W m^{-2} and 4 W m^{-2} (Skiles et al., 2012). By

comparison, in years like 2009 with high dust concentrations, daily mean enhanced surface shortwave absorption caused by dust in spring can be as high as 75 W m^{-2}, and even in the lowest dust concentration year, 2005, dust enhanced mean daily shortwave absorption by 27 W m^{-2}.

Concurrent studies project strong reductions in Colorado River runoff, with earlier snowmelt and melt-out dates due to reduced winter snowfall and warmer air temperatures (Barnett & Pierce, 2009; Christensen & Lettenmaier, 2007; Deems et al., 2013; Vano et al., 2012). To date, the relative and combined impacts of changes in temperature and dust radiative forcing (modulating albedo) on changes in the runoff hydrograph have been simulated over climatic time scales (Deems et al., 2013), but melt and runoff dynamics have not been studied with in situ observations on seasonal time scales. This void in understanding motivates our investigation of the signs and magnitudes of the energy balance forcings that affect this integrated signal. In particular, we test the dependence of interannual variability in mountain river hydrograph rising limb shape on interannual variability in spring air temperature and dust radiative forcing.

2.2 Data description

This study focuses on unimpeded flow from major rivers in the Colorado River Basin that carry primarily snowmelt from the western San Juan Mountains, Colorado (Figure 1), as measured by US Geological Survey gages (Tables S1 and S2). The four basins—Animas, Dolores, Uncompahgre, and the much smaller Senator Beck Basin—lie in the eastern half of the Upper Colorado River Basin. The Animas River flows southward past the gage at Silverton, CO to meet the San Juan River. The Dolores River flows southwest through the gage 6 km southwest of Rico, CO, joining the Colorado River near Moab, UT. The Uncompahgre River flows northward past the gage at Ridgway, CO with contributions from the Senator Beck Basin near the summit of Red Mountain Pass. The Senator Beck Stream Gage measures flow at 3362 m on the unnamed stream that drains the Senator Beck Basin Study Area .

The three larger basins drain the San Juan Mountains in three cardinal directions, representing a range of terrain aspect exposures. All basins consist of alpine and subalpine environments, with vegetation cover ranging from near non-existent in high alpine regions of the basins, which originate above 3800 m, to alpine meadows, coniferous (spruce/fir) forest, and in the three larger basins, deciduous trees near valley bottoms. The runoff hydrograph shapes describe typical snowmelt-dominated hydrologic systems. The onset of the rising limb is calculated here as the date on which the deviation from the running mean flow since January 1, or date of first measurement, exceeds 1% (Figure S2). Peak flow in these rivers generally occurs sometime during the second half of May and the first half of June.

The independent variables of air temperature and dust radiative forcing are derived from station measurements across the water years 2005 through 2014 at a well-instrumented site in the Senator Beck Basin Study Area (37°54’30”N, 107°43’30”W), in the headwaters of the Uncompahgre River (Landry et al., 2014; Painter et al., 2012b) and near the headwaters of the other basins. Changes in air temperatures influence the snow surface energy balance through two terms: sensible heating and longwave irradiance, the latter of which is also modulated by humidity (Marks & Dozier, 1992). Increased sensible heating and longwave heating from higher air temperatures should increase direct energy flux to the snowpack and increase snow grain size and decrease albedo, and in turn increase warming and melt.

We use the hourly estimates of at-surface radiative forcing by dust in snow *RF*, and positive degree days, *PDD*, calculated from air temperature ~2 m above the snow surface at

the Swamp Angel Study Plot. $\overline{RF}$ and $\overline{PDD}$ are defined as the average daily values over the period of the rising limb (d_0 to d_{end}), and the respective annual anomalies are subtractions of each year's mean value from the means of the annual values, where d is day of year and t is time:

$$\overline{RF} = \frac{1}{d_{end} - d_0} \int_{d_0}^{d_{end}} RF(t)dt \text{ and } \overline{PDD} = \frac{1}{d_{end} - d_0} \int_{d_0}^{d_{end}} PDD(t)dt \quad (1)$$

We evaluate the influence of air temperature and dust radiative forcing on the snowmelt hydrograph by determining the correlations for each year between the anomaly of the mean steepness of the rising limb $\overline{RL}$ and the $\overline{RF}$ and $\overline{PDD}$ anomalies. The rising limb slope is calculated as the slope of of the line connecting the onset of the rising limb to peak runoff, and is identical to the time averaged slope across all time steps of the rising limb. Further details on the methodology can be found in the supporting information (Cayan et al., 2001; Painter et al., 2012b; Skiles & Painter, 2016).

It is clear from the nonlinearity of the hydrographs (shallow rise early and then steeper rise later in reaching the peak runoff) that the distribution of slopes is skewed, due to the gradual nonlinear ramp up of the hydrograph. As such, we also characterize the hydrograph shape with three nonlinear metrics to attempt to account for any nonlinear effects in the slope calculation. The three metrics are μ, σ, and *BW*: The statistical distribution of the 1st derivative is usually lognormal, so it can be represented by parameters for scale μ (greater = steeper slope) and shape σ (greater = more variable slope). The distribution of the 2nd derivative is best represented by a kernel, a nonparametric representation of the probability density function that is defined by a smoothing function (in our case, normal) and a bandwidth *BW* that controls the smoothness of the resulting density curve.

3 Results

Hydrographs at each stream gage show marked interannual variability in the rising limb shapes (Figure 2). $\overline{RL}$ is uncorrelated with the peak flow and peak SWE magnitudes (Figure S3). In Figure 2, we color the rising limb slope traces according to each year's $\overline{RF}$ (left column) and $\overline{PDD}$ (right column). The coherent sequence of the color scale corresponding with the increasing magnitude of $\overline{RF}$ reveals qualitatively that the steepness of the rising limb varies directly with radiative forcing by dust in snow. Conversely, the colors of the traces are out of sequence with the increasing magnitude of $\overline{PDD}$, illustrating that the steepness of the rising limb is independent of degree-days.

The relationships between $\overline{RL}$ and $\overline{RF}$ range from 0.01 to 0.79 $m^3 d^{-1}$ per W m^{-2} with $0.70 \leq R^2 \leq 0.83$. Mean springtime $\overline{PDD}$ explains virtually none of the variance in $\overline{RL}$, with $0.0 \leq R^2 \leq 0.07$. Additionally, there is no correlation between $\overline{RL}$ anomalies and cumulative positive degree-day from 1 January, 1 February, or 1 March 1 (R^2=0.04, 0.04, and 0.03, respectively; all sites), indicating that temperatures preceding the onset of the rising limb (the warming of snowpack) are also very poor predictors of rising limb steepness.

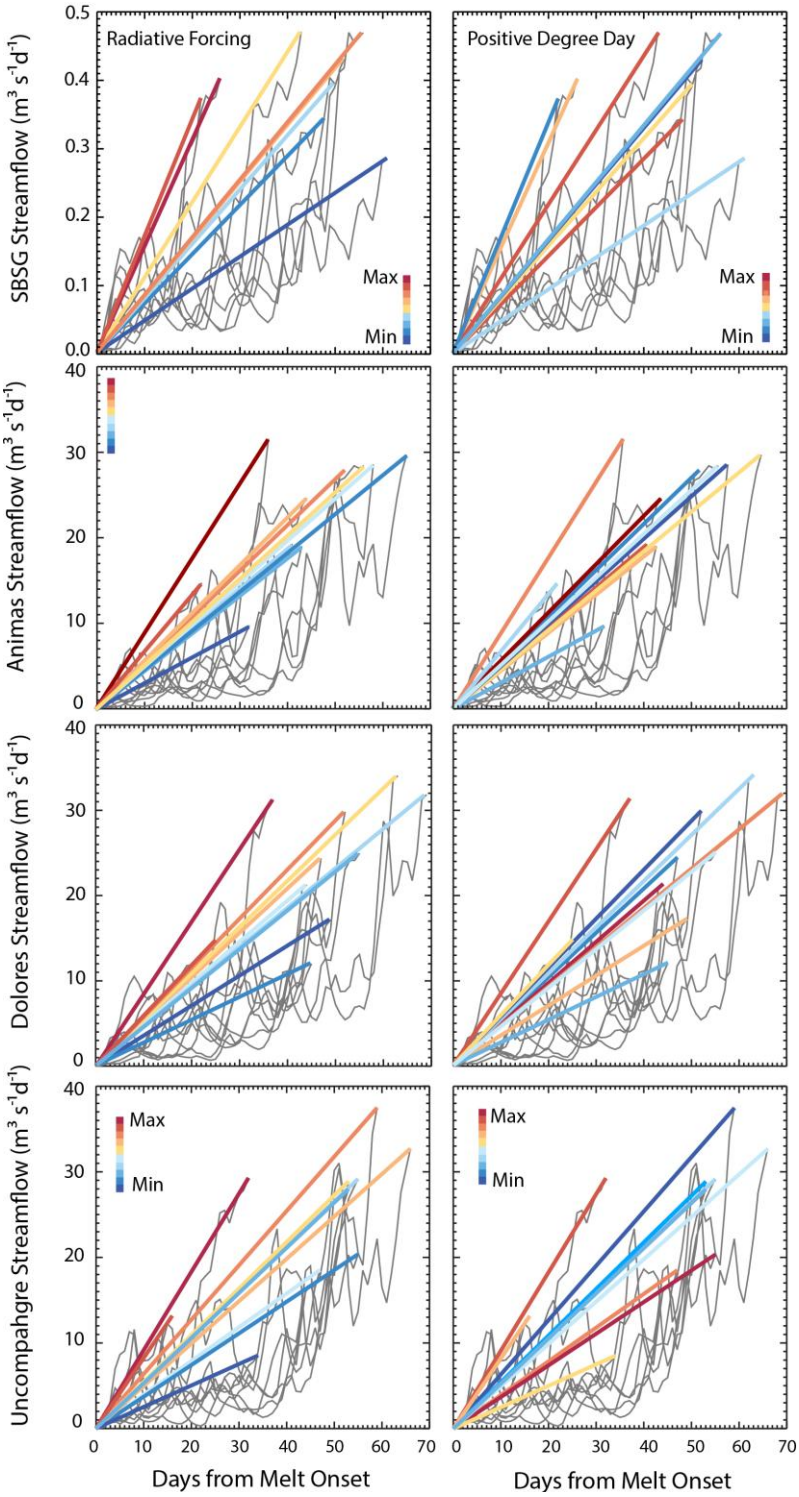

Figure 2. Hydrographs with mean slope from onset of rising limb to peak for each year in 2005-2014 for the four river basins. Left column is color coded according to $\overline{RF}$, showing that the radiative forcing coincides with the hydrograph steepness. Right column is color coded according to $\overline{PDD}$, showing that the hydrograph steepness is independent of degree-days.

To capture any effects due to the nonlinearity of most years' rising limbs that may not be adequately characterized by the linear slope, we assess the nonlinear metrics that characterize the hydrograph shape and relate those metrics to $\overline{RF}$ and $\overline{PDD}$. To illustrate that assessment, Figure 3a shows smoothed representations of the rising limb of the Animas River

for the two years with the highest radiative forcing and two with the lowest. The spline curves that approximate the rising limb, calculated by shape language modeling (D'Errico, 2017), are constrained to be monotonic and to go through the beginning and end of the rising limb. The 1st derivative of the smooth approximation to the rising limb displays a consistent shape, and the simple averages in Figure 2 do not completely express its distinctive attributes (Figure 3b). Instead, the statistical distributions of the 1st and 2nd derivatives of the rising limb can be represented by their probability density functions, as Figure 3c and d show. The 1st derivative is distributed lognormally, whereas the pdf of the 2nd derivative is best represented by a non-parametric kernel, with bandwidth *BW*.

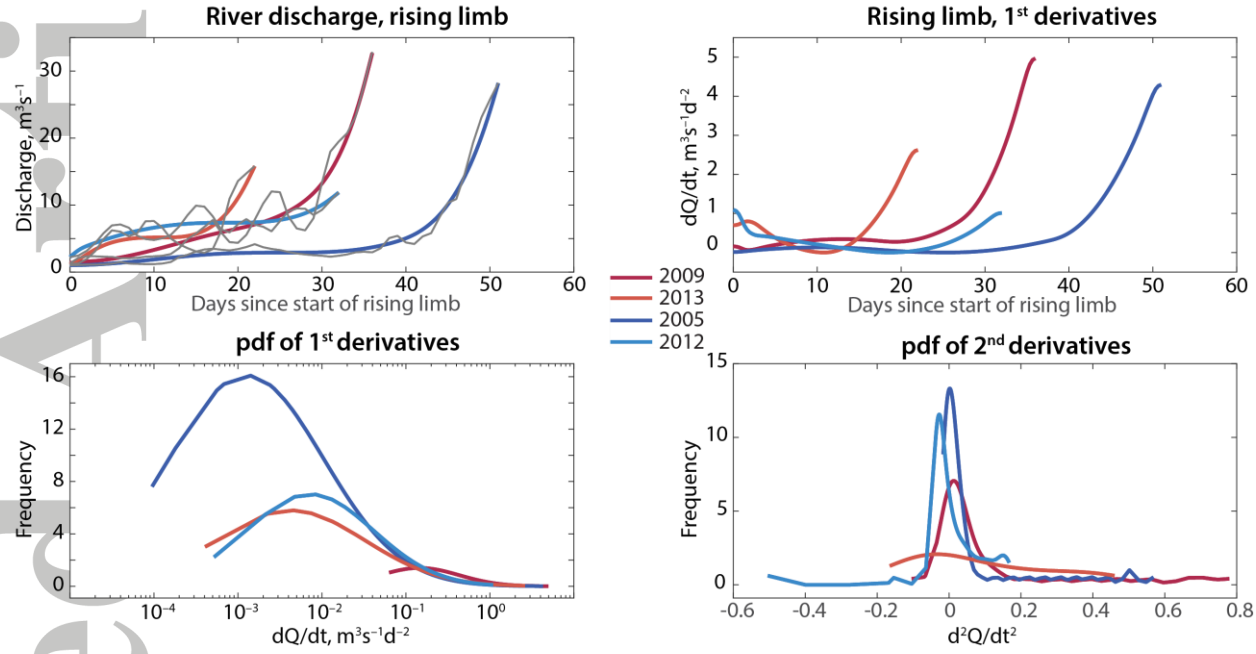

Figure 3. Characteristics to compare the rising limb with radiative and degree-day forcing of snowmelt. Color coding is the same as Figure 2. (**a**) Rising limb of the Animas River, with 2009 and 2013 the two years (out of ten) with the highest radiative forcing (*RF*), and 2005 and 2012 the two years with the lowest *RF*. (**b**) 1st derivative of the approximation, with the two years of the highest *RF* steepening earlier. The statistical distributions of the 1st derivatives are lognormal: (**c**) Probability distribution functions (pdf), with the years with higher *RF* peaking further to the right, i.e. with a greater μ value in the lognormal distribution. (**d**) Probability distributions of the 2nd derivatives generally show a narrower width for the years with lower *RF*, but the relationships are less strong in comparison to the 1st derivative.

The left column of Figure 4 shows the relationship between radiative forcing $\overline{RF}$ and both the rising limb anomaly and the scale parameter μ of the statistical distribution of its slope. The right column show the same information for the relationship of positive degree days $\overline{PDD}$ to the rising limb. In all four basins—Animas, Dolores, Senator Beck, and Uncompahgre—the relationships between the hydrograph shape and radiative forcing are statistically significant at the p=0.05 level, whereas the relationships with positive degree days are not statistically significant in any basin. Relationships between *RF* or *PDD* and the shape parameter σ of the statistical distribution are generally not significant. Relationships between *RF* and the kernel parameter of the 2nd derivative's kernel distribution are significant in three of the four basins (Table 1).

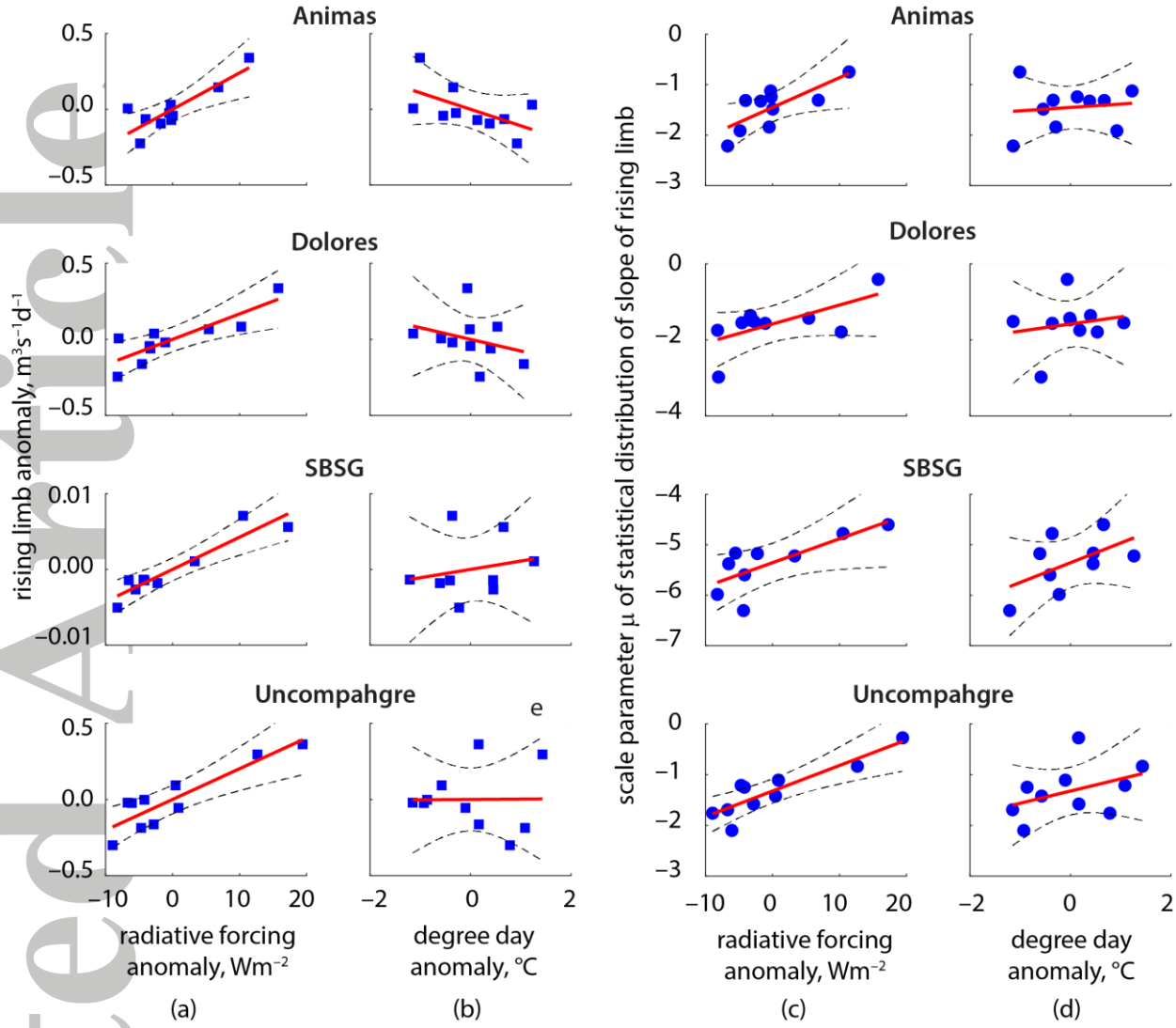

Figure 4. Scatter diagrams for the four basins showing the relationships between measures of hydrograph shape— $\overline{RL}$ anomaly in columns (**a**) and (**b**), statistical scale parameter μ in columns (**c**) and (**d**)—and the energy driver for snowmelt— radiative forcing $\overline{RF}$ in columns (**a**) and (**c**), positive degree days $\overline{PDD}$ in columns (**b**) and (**d**). In all basins, the confidence intervals on the linear fits show the relationships between *RF* and both the *RL* anomaly and μ are statistically significant at the *p*=0.05 level, whereas the relationships between *PDD* and the shape of the rising limb are not statistically significant in any basin.

Because both radiative forcing and degree-day forcings could influence snowmelt timing, we investigate these together. Regression results for $\overline{RL}$ predicted by $\overline{RF}$ and $\overline{PDD}$ illustrate the dominance of the radiative forcing on snowmelt, even in years with anomalously warm spring air temperatures (Table 1). The correlation coefficients for $\overline{RF}$ indicate strong predictive relationships, from a low of 0.85 (Dolores) to a high of 0.94 (SBSG), whereas the correlation coefficients for $\overline{PDD}$ span 0.0, from -0.57 (Animas) to +0.21 (SBSG). Adjusted R^2 values for $\overline{RF}$ range from 0.69 to 0.86, whereas for $\overline{PDD}$ they range from -0.12 to +0.24. Although the sample sizes are small, owing to the number of years for which radiative forcing information is available, the probabilities *p* of the null hypothesis and the adjusted R^2 values account for the sample size.

Table 1. Statistical parameters of the relationships shown in Figure 2 through Figure 4. Table S3 shows the uncertainty ranges for the Pearson correlation coefficients.

	ρ , Pearson correlation coefficient				*pr* , probability of null hypothesis				adjusted R^2	
	RF vs . . .				*RF* vs . . .				*RF* vs . . .	
basin	*RL*	μ	σ	*BW*	*RL*	μ	σ	BW	RL	μ
Animas	**0.86**	**0.75**	-0.24	0.45	**0.002**	**0.013**	0.496	0.193	**0.70**	**0.51**
Dolores	**0.85**	**0.63**	-0.09	**0.56**	**0.002**	**0.048**	0.790	**0.037**	**0.69**	**0.33**
SBSG	**0.94**	**0.76**	-0.03	**0.84**	**0.000**	**0.018**	0.933	**0.005**	**0.86**	**0.52**
Uncompahgre	**0.89**	**0.89**	-0.27	**0.75**	**0.001**	**0.001**	0.446	**0.007**	**0.77**	**0.76**
	PDD vs . . .				*PDD* vs . . .				*PDD* vs . . .	
	RL	μ	σ	*BW*	*RL*	μ	σ	*BW*	RL	μ
Animas	-0.57	0.13	-0.34	0.15	0.084	0.730	0.343	0.376	0.24	-0.11
Dolores	-0.30	0.19	-0.11	0.41	0.398	0.608	0.761	0.144	-0.02	-0.09
SBSG	0.21	0.55	-0.34	0.19	0.584	0.126	0.377	0.429	-0.09	0.20
Uncompahgre	0.01	0.41	-0.40	0.56	0.979	0.234	0.258	0.085	-0.12	0.07

bold: significant at the *pr* =0.05 level

The data in Table 1 also show that the scale parameter μ of the 1st derivative of the rising limb of the hydrograph is consistently correlated with the radiative forcing anomaly. In three of the four basins, the bandwidth parameter of the kernel distribution of the 2nd derivative is also correlated with the radiative forcing anomaly. The positive degree day anomaly correlates with no descriptor of the rising limb of the hydrograph in any of these snowmelt-dominated basins.

4 Discussion and conclusions

Dust radiative forcing so dominates the surface energy flux that snowmelt rates are insensitive to air temperatures over the rising limb of the hydrograph in the San Juan Mountains of the Colorado River Basin. Air temperatures are also driven by solar input, hence the utility of air temperature as a melt index parameter, but early in the melt season, despite RF-driven snowmelt, air temperatures remain suppressed by the presence of extensive snow cover, only increasing substantially as the lower elevations become snow-free. Thus, when averaged over the RF-shortened rising limb in our study basins, the positive degree-days exhibit no significant relationship with the metrics for the shape of the hydrograph's rising limb.

The impact of dust-induced shortening of the rising limb (Deems et al., 2013; Painter et al., 2010) is likely consuming important adaptive capacity in human and natural systems, where management adjustment to earlier or faster snowmelt runoff may not be resilient enough to accommodate impending hydroclimatic changes (Bryant et al., 2013). For example, in the extreme dust years of 2009 and 2013 in the Colorado Rocky Mountains, water distribution infrastructure was nearly destroyed due to unexpected, abrupt snowmelt pulses (Vandiver, 2009). In other mountainous regions where the magnitude of dust and black carbon forcing of snowmelt is powerful (Davitaya, 1969; Jenk et al., 2006; Kaspari et al., 2014; Lau et al., 2010; McConnell et al., 2007; Ming et al., 2013; Oerlemans et al., 2009; Painter et al., 2013a), this control on snowmelt runoff hydrographs is likely to be of similar or greater magnitude. For example, in the Himalaya, dust loading has increased four-fold since the 1850s (Thompson et al., 2000) and black carbon loading has increased 2.5-fold since the 1970s. Kaspari et al. (2014) found dust concentrations in the Solu-Khumbu reaching greater

than 28 pptw, markedly greater than the ~4 pptw in the Colorado Rocky Mountains (Painter et al., 2012b), and BC concentrations reaching greater than 3 ppmw, with inferred daily mean radiative forcings exceeding 150 W m^{-2}. Moreover, impurity concentrations at different annual layers had strong variability and as such likely cause strong interannual variability in radiative forcings, contributing to variability in snowmelt rates and flow.

An analysis of different climatic systems where impurities impact warming and melt would help shed light on the relative importance of temperature and radiative forcing in those systems. Likewise, as there are few detailed energy balance and radiation measurements like those in the Senator Beck Basin, subsequent study should include remote sensing retrievals such as the MODIS Dust Radiative Forcing in Snow (MODDRFS) (Painter et al., 2012a). More precise radiative forcing retrievals from the NASA Airborne Snow Observatory (Painter et al., 2016) and the NASA Airborne Visible/Infrared Imaging Spectrometer (AVIRIS) (Painter et al., 2013b; Seidel et al., 2016) will allow a broader scaling than will individual energy balance towers, if they exist.

We focus here on net solar radiation forcings in an effort to highlight potential vulnerabilities in conventional snowmelt simulation approaches reliant on air temperatures. However, under many hydroclimatic change trajectories, all components of the surface energy balance are subject to change, arguing even more strongly for incorporation of physical process representations in monitoring and modeling systems. While solar forcings are likely to remain dominant during spring melt seasons, a full treatment of snow energy balance sensitivity under combined hydroclimatic change trajectories (e.g., Deems et al., 2013) would be valuable. For example, recent work showing earlier and slower snowmelt in a warmer climate (Musselman et al., 2017) implies that though dust radiative forcing would remain the primary driver of steepness of the rising limb, rising limbs should be less steep when shifted earlier in the year.

Forecasts of snowmelt runoff by the National Weather Service's Colorado Basin River Forecast Center provide the primary flow estimates throughout the Colorado River Basin and Eastern Great Basin for a wide range of users, from small farmers and recreationalists to federal entities. The results here, along with the known sensitivity of forecast errors to dust radiative forcing (Bryant et al., 2013), suggest that knowledge of impurity forcings is needed for accurate flow forecasting. This observation tells us that temperature-index based guidance, whether operational or scientific, is vulnerable to radiation-driven variations in snowmelt processes.

In many western US states and river basins, water delivery obligations are bound by flow timing restrictions, with specific rights or diversions limited to specific date windows or keyed to the occurrence of peak flow (Kenney et al., 2008). Shifts in flow magnitude via steeper rising limbs induced by dust radiative forcing can thereby have important operational and political ramifications, and a “flashy” rising limb can complicate real-time identification of peak flow occurrence (Kenney et al., 2008). In contrast to global climate warming, dust production and deposition is primarily a regional problem, with the potential for tractable, regional solutions, reinforcing the importance of attribution of the source of earlier snowmelt runoff.

It is important to note here that anthropogenic climate change still poses a grave threat to sustainability of our water system, and this analysis by no means suggests otherwise. Regional warming in the mountains has its impact mainly through the change of phase of precipitation from snow to rain and secondarily through increase in temperature at which snow is deposited (thus reducing *cold content*, the energy required to bring the snowpack to the melting point) (DeWalle & Rango, 2008; Fyfe et al., 2017). The snow line will increase in

elevation and precipitation below that line will run off immediately rather than remaining in the implicit water reservoir of the snowpack. Moreover, warming will also increase evapotranspiration and reduce soil moisture earlier in the season. However, faster melt due to warming will continue to be overwhelmed, and compounded by dust forcing.

Acknowledgments and Data

We are grateful to Jeff Derry and Chris Landry, Center for Snow and Avalanche Studies, Silverton, CO. This work was funded by NASA project NNX10AO97G. Part of this work was performed at the Jet Propulsion Laboratory, California Institute of Technology under a contract with NASA. Part of this work was supported by the NOAA Climate Program Office through the Western Water Assessment RISA at CIRES, University of Colorado-Boulder.

All data used in the analysis are in the Supporting Information.

References

Barnett, T. P., Adam, J. C., & Lettenmaier, D. P. (2005). Potential impacts of a warming climate on water availability in snow-dominated regions. *Nature, 438*, 303-309. doi:10.1038/nature04141

Barnett, T. P., & Pierce, D. W. (2009). Sustainable water deliveries from the Colorado River in a changing climate. *Proc. Natl. Acad. Sci., 106*(18), 7334-7338. doi:10.1073/pnas.0812762106

Blöschl, G. (1991). The influence of uncertainty in air temperature and albedo on snowmelt. *Nordic Hydrol., 22*(2), 95-108.

Box, J. E., Fettweis, X., Stroeve, J. C., Tedesco, M., Hall, D. K., & Steffen, K. (2012). Greenland ice sheet albedo feedback: thermodynamics and atmospheric drivers. *The Cryosphere, 6*, 821-839. doi:10.5194/tc-6-821-2012

Brahney, J., Ballantyne, A. P., Sievers, C., & Neff, J. C. (2013). Increasing Ca2+ deposition in the western US: The role of mineral aerosols. *Aeolian Research, 10*, 77-87. doi:10.1016/j.aeolia.2013.04.003

Brubaker, K., Rango, A., & Kustas, W. (1996). Incorporating radiation inputs into the snowmelt runoff model. *Hydrol. Process., 10*(10), 1329-1343. doi:10.1002/(SICI)1099-1085(199610)10:10<1329::AID-HYP464>3.0.CO;2-W

Bryant, A. C., Painter, T. H., Deems, J. S., & Bender, S. M. (2013). Impact of dust radiative forcing in snow on accuracy of operational runoff prediction in the Upper Colorado River Basin. *Geophys. Res. Lett., 40*(15), 3945-3949. doi:10.1002/grl.50773

Cayan, D. R., Dettinger, M. D., Kammerdiener, S. A., Caprio, J. M., & Peterson, D. H. (2001). Changes in the onset of spring in the Western United States. *Bulletin of the American Meteorological Society, 82*, 399-415. doi:10.1175/1520-0477(2001)082<0399:CITOOS>2.3.CO;2

Christensen, N. S., & Lettenmaier, D. P. (2007). A multimodel ensemble approach to assessment of climate change impacts on the hydrology and water resources of the Colorado River Basin. *Hydrol. Earth Syst. Sci., 11*, 1417-1434. doi:10.5194/hess-11-1417-2007

D'Errico, J. (2017). SLM – Shape language modeling. MATLAB Central File Exchange. Retrieved from http://www.mathworks.com/matlabcentral/fileexchange/24443-slm-shape-language-modeling

Davitaya, F. F. (1969). Atmospheric dust content as a factor affecting glaciation and climatic change. *Ann. Assoc. Am. Geog., 59*(3), 552-560. doi:10.1111/j.1467-8306.1969.tb00690.x

Deems, J. S., Painter, T. H., Barsugli, J. J., Belnap, J., & Udall, B. (2013). Combined impacts of current and future dust deposition and regional warming on Colorado River Basin snow dynamics and hydrology. *Hydrol. Earth Syst. Sci., 10*, 6237-6275. doi:10.5194/hessd-10-6237-2013

DeWalle, D. R., & Rango, A. (2008). *Principles of Snow Hydrology*: Cambridge University Press.

Dozier, J. (2011). Mountain hydrology, snow color, and the fourth paradigm. *Eos, Transactions American Geophysical Union, 92*, 373-375. doi:10.1029/2011EO430001

Dunne, T., & Leopold, L. B. (1978). *Water in Environmental Planning*. San Francisco: W. H. Freeman.

Fyfe, J., Derksen, C., Mudryk, L., Flato, G., Santer, B., Swart, N., . . . Jiao, Y. (2017). Large near-term projected snowpack loss over the western United States. *Nature Communications*. doi:10.1038/NCOMMS14996

Hamlet, A. F., Mote, P. W., Clark, M. P., & Lettenmaier, D. P. (2005). Effects of temperature and precipitation variability on snowpack trends in the western United States. *Journal of Climate, 18*(21), 4545-4561.

Hansen, J., & Nazarenko, L. (2004). Soot climate forcing via snow and ice albedos. *Proc. Nat. Acad. Sci. USA, 101*(2), 423-428. doi:10.1073/pnas.2237157100

Hock, R. (2003). Temperature index melt modelling in mountain areas. *J Hydrol, 282*, 104-115. doi:10.1016/S0022-1694(03)00257-9

Hock, R. (2005). Glacier melt: a review of processes and their modelling. *Progress in Physical Geography, 29*(3), 362-391. doi:10.1191/0309133305pp453ra

Jenk, T. M., Szidat, S., Schwikowski, M., Gäggeler, H. W., Brütsch, S., Wacker, L., . . . Saurer, M. (2006). Radiocarbon analysis in an Alpine ice core: record of anthropogenic and biogenic contributions to carbonaceous aerosols in the past. *Atmospheric Chemistry and Physics, 6*, 5381-5390. doi:10.5194/acp-6-5381-2006

Kaspari, S. D., Schwikowski, M., Gysel, M., Flanner, M. G., Kang, S., Hou, S., & Mayewski, P. A. (2011). Recent increase in black carbon concentrations from a Mt. Everest ice core spanning 1860-2000 AD. *Geophys. Res. Lett., 38*, L04703. doi:10.1029/2010GL046096

Kaspari, S. D., Painter, T. H., Gysel, M., & Schwikowski, M. (2014). Spatial and seasonal variations in black carbon concentrations in snow and ice in the Solu-Khumbu, Nepal. *Atmospheric Chemistry and Physics, 14*, 8089-8103. doi:10.5194/acp-14-8089-2014

Kenney, D., Klein, R., Goemans, C., Alvord, C., & Shapiro, J. (2008). *The impact of earlier spring snowmelt on water rights and administration: A preliminary overview of issues and circumstances in the Western states*. Boulder, CO: Western Water Assessment. Retrieved from http://wwa.colorado.edu/publications/reports/WWA_Kenney_et_al_Snowmelt-WaterRights_2008.pdf

Kirnbauer, R., Blöschl, G., & Gutknecht, D. (1994). Entering the era of distributed snow models. *Nord. Hydrol., 25*(1-2), 1-24.

Kumar, M., Marks, D., Dozier, J., Reba, M., & Winstral, A. (2013). Evaluation of distributed hydrologic impacts of temperature-index and energy-based snow models. *Adv. Water Resour., 56*, 77-89. doi:10.1016/j.advwatres.2013.03.006

Kustas, W. P., & Rango, A. (1994). A simple energy budget algorithm for the snowmelt runoff model. *Water Resour. Res., 30*(5), 1515-1527. doi:10.1029/94WR00152

Landry, C. C., Buck, K. A., Raleigh, M. S., & Clark, M. P. (2014). Mountain system monitoring at Senator Beck Basin, San Juan Mountains, Colorado: A new integrative data source to develop and evaluate models of snow and hydrologic processes. *Water Resour. Res., 50*, 1773-1788. doi:10.1002/2013WR013711

Lau, K. M., Kim, M. K., Kim, K. M., & Lee, W. S. (2010). Enhanced surface warming and accelerated snow melt in the Himalayas and Tibetan Plateau induced by absorbing aerosols. *Environ. Res. Lett., 5*, 025204. doi:10.1088/1748-9326/5/2/025204

Mankin, J. S., Viviroli, D., Singh, D., Hoekstra, A. Y., & Diffenbaugh, N. S. (2015). The potential for snow to supply human water demand in the present and future. *Environ. Res. Lett., 10*(11), 114016. doi:10.1088/1748-9326/10/11/114016

Marks, D., & Dozier, J. (1992). Climate and energy exchange at the snow surface in the alpine region of the Sierra Nevada 2. Snow cover energy balance. *Water Resour. Res., 28*(11), 3043-3054.

McConnell, J. R., Aristarain, A. J., Banta, J. R., Edwards, P. R., & Simoes, J. C. (2007). 20th-Century doubling in dust archived in an Antarctic Peninsula ice core parallels climate change and desertification in South America. *Proc. Natl. Acad. Sci., 104*(14), 5743-5748. doi:10.1073/pnas.0607657104

Milly, P. C. D., Betancourt, J., Falkenmark, M., Hirsch, R. M., Kundzewicz, Z. W., Lettenmaier, D. P., & Stouffer, R. J. (2008). Stationarity is dead: Whither water management? *Science, 319*, 573-574. doi:10.1126/science.1151915

Ming, J., Xiao, C., Du, Z., & Yang, X. (2013). An overview of black carbon deposition in High Asia glaciers and its impacts on radiation balance. *Adv. Water Resour., 55*, 80-87. doi:10.1016/j.advwatres.2012.05.015

Musselman, K. N., Clark, M. P., Liu, C., Ikeda, K., & Rasmussen, R. (2017). Slower snowmelt in a warmer world. *Nature Climate Change, 7*, 214-219. doi:10.1038/nclimate3225

Nair, V. S., Babu, S. S., Moorthy, K. K., Sharma, A. K., Marinoni, A., & Ajai. (2013). Black carbon aerosols over the Himalayas: direct and surface albedo forcing. *Tellus, Series B Chemical and Physical Meteorology, 65*(19738), 1-14. doi:10.3402/tellusb.v65i0.19738

Neff, J. C., Ballantyne, A. P., Farmer, G. L., Mahowald, N. M., Conroy, J. L., Landry, C. C., . . . Reynolds, R. L. (2008). Increasing eolian dust deposition in the western United States linked to human activity. *Nature Geosci., 1*, 189-195. doi:10.1038/ngeo133

Oerlemans, J. (2000). Analysis of a 3 year meteorological record from the ablation zone of Morteratschgletscher, Switzerland: energy and mass balance. *J. Glaciol., 46*(155), 571-579. doi:10.3189/172756500781832657

Oerlemans, J., Giesen, R. H., & Van den Broeke, M. R. (2009). Retreating alpine glaciers: increased melt rates due to accumulation of dust (Vadret da Morteratsch, Switzerland). *J. Glaciol., 55*(192), 729-736.

Painter, T. H., Barrett, A. P., Landry, C. C., Neff, J. C., Cassidy, M. P., Lawrence, C. R., . . . Farmer, G. L. (2007). Impact of disturbed desert soils on duration of mountain snow cover. *Geophys. Res. Lett., 34*, L12502. doi:10.1029/2007GL030284

Painter, T. H., Rittger, K., McKenzie, C., Slaughter, P., Davis, R. E., & Dozier, J. (2009). Retrieval of subpixel snow covered area, grain size, and albedo from MODIS. *Remote Sensing of Environment, 113*, 868-879. doi:10.1016/j.rse.2009.01.001

Painter, T. H., Deems, J. S., Belnap, J., Hamlet, A. F., Landry, C. C., & Udall, B. (2010). Response of Colorado River runoff to dust radiative forcing in snow. *Proc. Nat. Acad. Sci. USA, 107*(40), 17125-17130. doi:10.1073/pnas.0913139107

Painter, T. H., Bryant, A. C., & Skiles, S. M. (2012a). Radiative forcing of dust in mountain snow from MODIS surface reflectance data. *Geophys. Res. Lett., 39*(L17502). doi:10.1029/2012GL052457

Painter, T. H., Skiles, S. M., Deems, J. S., Bryant, A. C., & Landry, C. C. (2012b). Dust radiative forcing in snow of the Upper Colorado River Basin: Part I. A 6 year record of energy balance, radiation, and dust concentrations. *Water Resour. Res., 48*(7), W07521. doi:10.1029/2012WR011985

Painter, T. H., Flanner, M., Marzeion, B., Kaser, G., VanCuren, R., & Abdalati, W. (2013a). End of the Little Ice Age in the Alps forced by black carbon. *Proc. Natl. Acad. Sci., 110*(38), 15216-15221. doi:10.1073/pnas.1302570110

Painter, T. H., Seidel, F., Bryant, A. C., Skiles, S. M., & Rittger, K. (2013b). Imaging spectroscopy of albedo and radiative forcing by light absorbing impurities in mountain snow. *J. Geophys. Res., 118*(17), 9511-9523. doi:10.1029/2012JD019398

Painter, T. H., Berisford, D. F., Boardman, J. W., Bormann, K. J., Deems, J. S., Gehrke, F., . . . Winstral, A. (2016). The Airborne Snow Observatory: scanning lidar and imaging spectrometer fusion for mapping snow water equivalent and snow albedo. *Remote Sensing of Environment, 184*, 139-152. doi:10.1016/j.rse.2016.06.018

Seidel, F. C., Rittger, K., Skiles, S. M., Painter, T. H., & Molotch, N. P. (2016). Case study of spatial and temporal variability of snow cover, grain size, albedo, and radiative forcing in the Sierra Nevada and Rocky Mountain snowpack derived from imaging spectroscopy. *The Cryosphere, 10*, 1229-1244. doi:10.5194/tc-2015-196

Skiles, S. M., Painter, T. H., J. S. Deems, Bryant, A. C., & Landry, C. C. (2012). Dust radiative forcing in snow of the Upper Colorado River Basin: Part II. Interannual variability in radiative forcing and snowmelt rates. *Water Resour. Res., 48*(7), W07522. doi:10.1029/2012WR011986

Skiles, S. M., & Painter, T. H. (2016). Daily evolution in dust and black carbon content, snow grain size, and snow albedo during snowmelt, Rocky Mountains, Colorado. *J. Glaciol., 63*(237), 118-132. doi:10.1017/jog.2016.125

Tedesco, M., Fettweis, X., van den Broeke, M. R., Wal, R. S. W. v. d., Smeets, C. J. P. P., van de Berg, W. J., . . . Box, J. E. (2011). The role of albedo and accumulation in the 2010 melting record in Greenland. *Environ. Res. Lett., 6*(1), 014005. doi:10.1088/1748-9326/6/1/014005

Thompson, L. G., Yao, T., Mosley-Thompson, E., Davis, M. E., Henderson, K. A., & Lin, P.-N. (2000). A high-resolution millennial record of the south Asian monsoon from Himalayan ice cores. *Science, 289*, 1916-1919. doi:10.1126/science.289.5486.1916

Van den Broeke, M. R., Van De Wal, R., & Smeets, P. (2011). The seasonal cycle and interannual variability of surface energy balance and melt in the ablation zone of the west Greenland ice sheet. *Cryosphere, 5*, 779-809. doi:10.5194/tc-5-377-2011

Vandiver, S. (2009).

Vano, J. A., Das, T., & Lettenmaier, D. P. (2012). Hydrologic sensitivities of Colorado River Runoff to changes in precipitation and temperature. *J. Hydrometeorol., 13*, 932-949. doi:10.1175/JHM-D-11-069.1

Warren, S. G., & Wiscombe, W. J. (1980). A model for the spectral albedo of snow, II, Snow containing atmospheric aerosols. *J. Atmos. Sci., 37*(12), 2734-2745. doi:10.1175/1520-0469(1980)037<2734:AMFTSA>2.0.CO;2

Warren, S. G., & Brandt, R. E. (2008). Optical constants of ice from the ultraviolet to the microwave: A revised compilation. *J. Geophys. Res., 113*, D14220. doi:10.1029/2007JD009744

Wiscombe, W. J., & Warren, S. G. (1980). A model for the spectral albedo of snow, I, Pure snow. *J. Atmos. Sci., 37*(12), 2712-2733. doi:10.1175/1520-0469(1980)037<2712:AMFTSA>2.0.CO;2

Woodhouse, C. A., Gray, S. T., & Meko, D. M. (2006). Updated streamflow reconstructions for the Upper Colorado River Basin. *Water Resour. Res., 42*, W05415. doi:10.1029/2005WR2005WR004455

Yasunari, T. J., Tan, Q., Lau, K.-M., Bonasoni, P., Marinoni, A., Laj, P., . . . Chin, M. (2013). Estimated range of black carbon dry deposition and the related snow albedo reduction over Himalayan glaciers during dry pre-monsoon periods. *Atmos. Environ., 78*, 259-267. doi:10.1016/j.atmosenv.2012.03.031